Kuwabara, Y., Ichiya, Y., Sasaki, M., Yoshida, T., Masuda, K., Matsushima, T. & Fukui, M. 1997. Response to hypercapnia in moyamoya disease. Cerebrovascular response to hypercapnia in pediatric and adult patients with moyamoya disease. *Stroke* **28**, 701-707.

Love, WD., Tyler, MD., Abraham, RE. & Munford, RS. 1965. Effects of O2, CO2, and drugs on estimating coronary blood flow from Rb86 clearance. *Am J Physiol* **208**, 1206-1210.

Neill, WA. & Hattenhauer, M. 1975. Impairment of myocardial O2 supply due to hyperventilation. *Circulation* **52**, 854-858.

Powers, ER., Bannerman, KS., Fitz-James, I., & Cannon, PJ. 1986. Effect of elevations of coronary artery partial pressure of carbon dioxide (PCO2) on coronary blood flow. *J Am Coll Cardiol* **8**, 1175-1181.

Raichle, ME., Martin, WRW., Herscovitch, P., Mintun, MA., & Markham, J. 1983. Brain blood flow measured with intravenous H2(15)O. II. Implementation and validation. *J Nucl Med* **24**, 790-798.

Rowe, GG., Castillo, CA. & Crumpton, CW. 1962. Effects of hyperventilation on systemic and coronary hemodynamics. *Am Heart J* **63**, 67-77.

Shimosegawa, E., Kanno, I., Hatazawa, J., Fujita, H., Iida, H., Miura, S., Murakami, M., Inugami, A., Ogawa, T., Itoh, H., Okudera, T. & Umemura, K. 1995. Photic stimulation study of changing the arterial partial pressure level of carbon dioxide. *J Cereb Blood Flow Metab* **15**, 111-114.

van den Bos, GC., Drake, AJ. & Noble, MI. 1979. The effect of carbon dioxide upon myocardial contractile performance, blood flow and oxygen consumption. *J Physiol* **287**, 149–162.

Wilson, JR., Goldberg, S., Hirshfeld, JW. & Harken, AH. 1981. Effects of respiratory alkalosis on coronary vascular dynamics and myocardial energetics in patients with coronary artery disease. *Am Heart J* **102**, 202-205.

Table 1. Hemodynamics, arterial carbon dioxide tension and pH during $H_2{}^{15}O$ PET studies

	Rest	Hypercapnea	Hypocapnea
Systolic blood pressure (mmHg)	146.5 ±20.9	159.8 ±25.4	144.8 ±26.7
Diastolic blood pressure (mmHg)	82.8 ±12.0	85.3 ±10.7	78.5 ±13.2
Heart rate (beat / minute)	58.4 ±7.8	61.6 ±8.7	60.7 ±7.8
Rate pressure product	8472 ±1146	9758 ±1609	8717 ±1677
Arterial carbon dioxide tension	40.2 ±2.4	43.1 ±2.7* $	29.2 ±3.4† $
pH	7.417 ±0.013	7.385 ±0.019 $	7.505 ±0.039 $

Data are presented as mean ± standard deviation.

Significance of changes compared with the three groups: *P<0.05, †P<0.01 by Fisher PLSD, Significance of changes compared with the resting condition: P<0.05, $ P < 0.01 by Wilcoxon signed rank test

Table 2. Cerebral blood flow ($mL*minute^{-1}*[100\ gram\ of\ perfusable\ tissue]^{-1}$), myocardial blood flow ($mL*minute^{-1}*[100\ gram\ of\ perfusable\ tissue]^{-1}$), and normalized myocardial blood flow ($100mL*mmHg^{-1}*[heart\text{-}beat]^{-1}*[gram\ of\ perfusable\ tissue]^{-1}$)

	Rest	Hypocapnea	Hypercapnea
Cerebral blood flow	39.8 ±5.3	27.0 ±6.3†	48.4 ±10.4*
Myocardial blood flow	78.2 ±12.6	55.1 ±14.6†	88.7 ±22.4
Normalized myocardial blood flow	93.4 ±16.6	64.5 ±18.3†	90.5 ±14.3

Significance of changes compared with the three groups: *$P < 0.05$, †$P < 0.01$

Eur J Nucl Med Mol Imaging
DOI 10.1007/s00259-007-0654-4

ORIGINAL ARTICLE

Absolute quantitation of myocardial blood flow with ^{201}Tl and dynamic SPECT in canine: optimisation and validation of kinetic modelling

Hidehiro Iida · Stefan Eberl · Kyeong-Min Kim · Yoshikazu Tamura · Yukihiko Ono · Mayumi Nakazawa · Antti Sohlberg · Tsutomu Zeniya · Takuya Hayashi · Hiroshi Watabe

Received: 18 September 2007 / Accepted: 4 November 2007

Abstract
Purpose ^{201}Tl has been extensively used for myocardial perfusion and viability assessment. Unlike ^{99m}Tc-labelled agents, such as ^{99m}Tc-sestamibi and ^{99m}Tc-tetrofosmine, the regional concentration of ^{201}Tl varies with time. This study is intended to validate a kinetic modelling approach for in vivo quantitative estimation of regional myocardial blood flow (MBF) and volume of distribution of ^{201}Tl using dynamic SPECT.
Methods Dynamic SPECT was carried out on 20 normal canines after the intravenous administration of ^{201}Tl using a commercial SPECT system. Seven animals were studied at rest, nine during adenosine infusion, and four after beta-blocker administration. Quantitative images were reconstructed with a previously validated technique, employing OS-EM with attenuation-correction, and transmission-dependent convolution subtraction scatter correction. Measured regional time–activity curves in myocardial segments were fitted to two- and three-compartment models. Regional MBF was defined as the influx rate constant (K_1) with corrections for the partial volume effect, haematocrit and limited first-pass extraction fraction, and was compared with that determined from radio-labelled microspheres experiments.
Results Regional time–activity curves responded well to pharmacological stress. Quantitative MBF values were higher with adenosine and decreased after beta-blocker compared to a resting condition. MBFs obtained with SPECT (MBF_{SPECT}) correlated well with the MBF values obtained by the radio-labelled microspheres (MBF_{MS}) ($MBF_{SPECT}=-0.067+1.042\times MBF_{MS}$, $p<0.001$). The three-compartment model provided better fit than the two-compartment model, but the difference in MBF values between the two methods was small and could be accounted for with a simple linear regression.
Conclusion Absolute quantitation of regional MBF, for a wide physiological flow range, appears to be feasible using ^{201}Tl and dynamic SPECT.

Keywords Myocardial blood flow · Dynamic SPECT · Thallium-201 · Compartment model · Quantitation

H. Iida (✉) · S. Eberl · K.-M. Kim · M. Nakazawa · A. Sohlberg · T. Zeniya · T. Hayashi · H. Watabe
Department of Investigative Radiology,
National Cardiovascular Center Research Institute,
Fujishiro-dai,
Suita City, Osaka 565-8565, Japan
e-mail: iida@ri.ncvc.go.jp

S. Eberl
PET and Nuclear Medicine Department,
Royal Prince Alfred Hospital,
Missenden Road,
Camperdown, NSW 2050, Australia

Y. Tamura
Department of Cardiology, Akita Kumiai General Hospital,
1-1-1, Nishi-bukuro, Iijima,
Akita City 011-0948, Japan

Y. Ono
Akita Research Institute of Brain,
6-10, Senshu-Kubota Machi,
Akita City 010-0874, Japan

Introduction

Myocardial perfusion imaging using Thallium-201 (^{201}Tl) is well established in routine clinical practice for detecting

exercise-induced myocardial ischaemia and/or for assessing myocardial viability in patients with coronary artery disease. The diagnosis, however, has been limited to qualitative or visual assessment of the physical extent of the defect areas rather than quantitative assessment of physiological functions. Quantitative methods would for example enable longitudinal studies when assessing therapy response and pharmacological interventions. Some groups have already investigated the feasibility of estimating quantitative parameters with dynamic SPECT in the myocardium using ^{201}Tl [1] and ^{99m}Tc-Teboroxime [1, 2], but these techniques have not yet been applied to clinical practice. This is largely attributed to the fact that quantitative reconstruction programmes are not readily available on commercial SPECT systems.

We have developed a reconstruction programme package for SPECT, which can accurately provide quantitative images of radio-labelled tracer distributions in vivo, which is a pre-requisite for absolute physiological parameter estimation. The adequacy and accuracy of these methods have been demonstrated in multiple papers for ^{99m}Tc and ^{201}Tl in cardiac studies [3–5], and for ^{99m}Tc and ^{123}I in brain studies [6]. It has also been demonstrated, in brain studies, that physiological parameters such as cerebral perfusion [6] and cerebral flow reactivity [7] obtained using our package were as accurate as those determined by PET. These findings suggest that absolute quantitation of regional myocardial perfusion might also be possible in a clinical setting using commercial SPECT cameras.

^{201}Tl is a potassium analogue, and its kinetics has been extensively investigated in previous studies [8, 9]. Due to the high first-pass extraction fraction (EF) [10] and a large distribution volume, ^{201}Tl has been considered an ideal tracer for quantitation of absolute myocardial blood flow, not only at rest but also at hyperemic conditions. As a clinical implication, quantitative assessment of MBF and coronary flow reserve is important. For instance, coronary microvascular dysfunction or impaired endothelial function in patients with coronary risk factors or patients with cardiomyopathy or with heart failure is an un-resolved important issue to answer [11]. Coronary flow reserve can also be reduced in patients with hyper-cholesterolemia without overt coronary stenosis [12]. The low energy and long half-life of ^{201}Tl have, however, seriously limited its use in nuclear cardiology.

The goal of this study was to validate our reconstruction methodology for the estimation of myocardial blood flow using ^{201}Tl and dynamic SPECT using tissue time–activity curves (TTAC) derived from myocardial regions. In addition, we aimed to find the optimal kinetic model configuration and to investigate the factors affecting the estimation of physiological parameters such as the partial volume effect (PVE), appropriate choice of input function, conversion from plasma to blood flow using haematocrit (Hct) and the limited first-pass tracer EF.

Materials and methods

Subjects

A total of 21 dogs were studied in which 8 were in a resting condition, 9 dogs during constant infusion of adenosine for increased MBF, and 4 dogs during constant infusion of beta-blocker. Of the 21 studies, 1 study was un-successful and projection data could not be retrieved from the scanner, reducing the number of resting studies to 7 and total dog studies to 20. Adenosine was infused continuously over the study duration at a rate ranging from 140 to 700 mg/kg/h to achieve a range of blood flow increases. An initial dose of beta-blockers ranging from 2 to 6 mg was given, followed by a constant infusion for the duration of the study of 2 or 4 mg/h. The study protocol was approved by the animal ethics committee at the Akita Research Institute of Brain, Akita City, Japan where all experiments were carried out.

SPECT procedures

All dogs were anaesthetised, and the catheters for dose administration and arterial blood sampling were inserted before the study. The SPECT system was a conventional dual-head gamma camera (Toshiba GCA-7200A, Tokyo, Japan) fitted with short focal length fan-beam collimators (LEHR-Fan). The transverse field-of-view (FOV) was 22 cm diameter and axial FOV was 20 cm. The dogs were carefully taped into a cradle to minimise motion during the study, and also to ensure that no truncation occurred. Heart rate and blood pressure were monitored throughout the study and recorded at regular intervals.

Before the injection of any tracer, a 15-min transmission study was carried out in which a rod source filled with approximately 740 MBq of ^{99m}Tc was placed along the focal line of one of the fan-beam collimators (see Fig. 1). The transmission study was followed by injection of 3 MBq of ^{141}Ce microspheres into the left ventricle via a catheter and blood was withdrawn from the aorta at a constant flow rate of 5 ml/min for 2 min to serve as an input function. For the pharmacological intervention studies, adenosine infusion or beta-blocker injection followed by infusion was commenced before the ^{141}Ce microsphere administration.

Dynamic SPECT was commenced with the start of the 4-min constant infusion of 110 MBq ^{201}Tl. The frame collection rates and 360° rotation times were 10×1 min (rotation time 15 s), 6×2 min (30 s), 3×4 min (60 s) and 5×5 min (60 s) for the first hour for all studies. Resting blood flow studies had an additional 18×10 min (120 s) frames collected for a total study period over 4 h. The shorter total study time for the drug infusion studies was mandated by the difficulties in keeping the dogs stable with prolonged infusions of the drugs used. A 34% energy

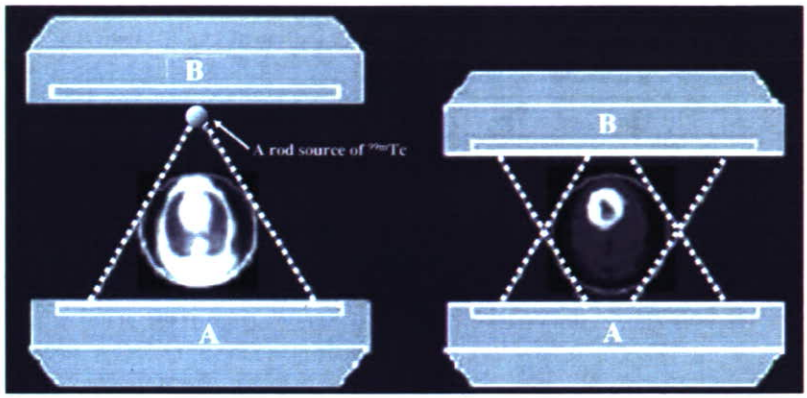

Fig. 1 Schematic diagram of data acquisition using a clinical dual-headed SPECT camera fitted with fan-beam collimators. Transmission scan was performed using a ^{99m}Tc-filled rod source placed at a focal line of one of the collimators, and only one of the detectors was used (*left*). Both detectors were used in the emission scan (*right*)

window centred on 77 keV was used for the ^{201}Tl acquisitions [4, 13].

Arterial blood samples were taken every 20 s for the first 6 min, every 60 s for 6–10 min, 120 s for 10–20 min, 300 s for 20–30 min and 600 s for 30–60 min. For the resting studies, blood samples were also taken every 20 min for 1–2 h and additional samples at 2.5, 3 and 4 h post-^{201}Tl infusion. In six studies, plasma was separated immediately after sampling by centrifugation, and plasma samples were counted in a well counter cross-calibrated with the SPECT scanner. To minimise the effects of the continued exchange of ^{201}Tl between plasma and red blood cells in the test tubes after sampling, immediate, rapid separation of plasma from whole blood was required. An averaged relationship between plasma and whole blood concentration ratio over time was obtained, and then multiplied with the whole blood curves for all studies to derive a plasma input function.

At the end of the SPECT study, the microsphere blood flow measurement was repeated with ^{51}Cr microspheres. The dogs were then killed by injection of potassium chloride (KCl) and the myocardium was dissected into samples suitable for counting in the well counter. The ^{201}Tl concentration in the tissue samples was derived from the sample weight normalised gamma counter counts. The samples were stored to allow for the decay of ^{201}Tl ($T_{1/2}$= 73 h vs $T_{1/2}$=32.5 days for ^{141}Ce and 27.8 days for ^{51}Cr) and then counted to measure the ^{141}Ce and ^{51}Cr activities. Separation between ^{141}Ce and ^{51}Cr counts was based on their respective gamma ray energies (145 keV for ^{141}Ce and 323 keV for ^{51}Cr).

SPECT data processing

Projection data were processed according to previously described procedures [5]. Briefly, the transmission data obtained by the fan-beam collimator were first re-binned into parallel projections. Transmission projections were normalised by blank projection, re-constructed to generate quantitative maps of the attenuation coefficient for ^{99m}Tc and then linearly scaled to provide attenuation correction maps for ^{201}Tl. Emission data were corrected for detector non-uniformity and also re-binned into parallel projections. The projection data were then corrected for scatter with transmission-dependent convolution subtraction (TDCS) originally proposed by Meikle et al. [14] and further optimised by our group [4, 5]. The emission projection data were re-constructed with the OS-EM reconstruction algorithm [15] using three iterations and ten subsets. The re-constructed images were cross-calibrated with the well counter system.

Data analysis

Re-constructed images were normalised by acquisition time for each frame. Multiple circular regions of interest (ROI) were drawn on the myocardium, and the TTAC of ^{201}Tl were generated for the anterior, apical, lateral, posterior and septal areas of the myocardium. The two-compartment model (one tissue compartment) and three-compartment model (two tissue compartments) shown in Fig. 2 were applied to determine two parameters (K_1 and K_2) for the two-compartment model and four parameters (K_1–K_4) for the three-compartment model by means of non-linear least squares fitting (NLLSF).

The regional MBF was considered to be related to K_1 obtained from compartment model fits. K_1 is, however, affected by the PVE, Hct and the limited first-pass EF whose effects were corrected according to Eq. 1:

$$\mathrm{MBF} = \frac{\mathrm{PVE}}{\mathrm{EF} \times (1 - \mathrm{Hct})} \times K_1 \qquad (1)$$

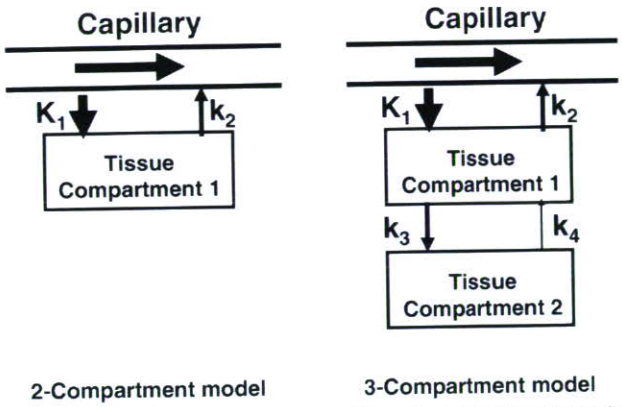

Fig. 2 Two- and three-compartment models evaluated in this study. K_1 in units of ml/min/g denotes the regional MBF for both models. Distribution volume (V_d) in units of ml/g is defined as K_1/K_2 for the two-compartment mode, and $\frac{K_1}{k_2}\left(1+\frac{k_3}{k_4}\right)$ for the three-compartment model

The physiological basis for the correction factors in Eq. 1 can be described as follows:

1. TTACs obtained from SPECT images are under-estimated due to the limited spatial resolution relative to the myocardial wall thickness and also due the myocardial contractile motion. This phenomenon is known as PVE. The PVE correction factor for each TTAC was determined from the ratio of the last SPECT frame counts to the ^{201}Tl myocardial tissue sample counts obtained from the tissue samples taken and measured with the well counter at the end of the SPECT scan.
2. The arterial input function for the compartment model studies was defined from the plasma radioactivity concentration curve, rather than the whole blood radioactivity curve. K_1 is therefore the regional "plasma" flow. Thus, for comparison with the microsphere flow measurements, which estimates the whole blood flow, K_1 was divided by (1−Hct) to obtain the flow for the total blood.
3. For a tracer with limited first-pass EF<1.0, flow (MBF) is related to K_1 by K_1=EF×MBF. The first-pass EF is flow-dependent and decreases at high flow. We have applied an empirical formulation for the first-pass EF based on the data by Weich et al. [10] (EF=0.84−0.524·$\log_{10}(K_1^*)$ where K_1^* is $K_1/(1-\text{Hct})$. The K_1 values obtained with two- and three-compartment models with/without corrections according to Eq. 1 were compared to the average of microsphere blood flow values obtained pre- and post-dynamic SPECT scan.

The distribution volume of ^{201}Tl (V_d) was defined as

$$V_d = \frac{K_1}{k_2} \text{ for the two} - \text{compartment model} \quad (2a)$$

$$V_d = \frac{K_1}{K_2}\left(1+\frac{K_3}{K_4}\right) \text{ for the three} - \text{compartment model.} \quad (2b)$$

As mentioned before, the resting studies were collected for 4 h, whilst the adenosine and beta-blocker studies were collected for approximately 1 h. To investigate whether the shorter collection time introduces systematic bias, NLLSF fits restricted to the first 1 h of the resting study data were also performed and compared with the V_d values from the full 4 h resting data set and with the estimates obtained from the beta-blocker and adenosine studies.

Akaike information criterion (AIC) and Schwarz criterion (SC) were calculated for both two-compartment and three-compartment model fits [16] to test the adequacy of the two models. All data are presented as mean±1 SD. Student's t test was employed in the comparison of the V_d values. Pearson's regression analysis was applied to compare K_1 and microsphere flow values. A probability value of <0.05 was considered statistically significant.

Results

Figure 3 shows the plasma to whole blood concentration ratios in the six dogs with rapid plasma separation and the averaged data. Equilibrium is reached after about 40 min, at which time the mean ratio was found to be 0.76. As expected, relative plasma concentration is highest early on as the tracer is injected into the plasma (and not red blood cells). ^{201}Tl is rapidly cleared from the plasma causing a rapid decline in relative plasma concentration and "undershoot" before equilibrium is established. Samples left for a prolonged period before plasma separation showed the value of approximately 0.78, which was close to the plasma to whole blood concentrations ratio at the equilibrium shown in

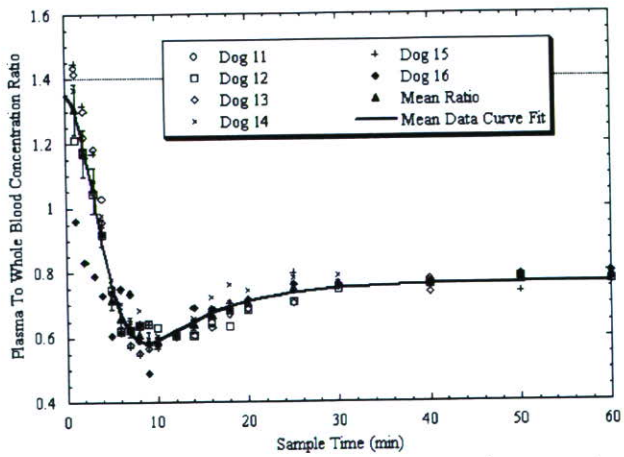

Fig. 3 Individual and mean plasma to whole blood concentration ratios over time for the six dogs with rapid plasma separation. *Error bars* indicate the standard error of the mean. *Solid line* is the curve fit to mean ratio data

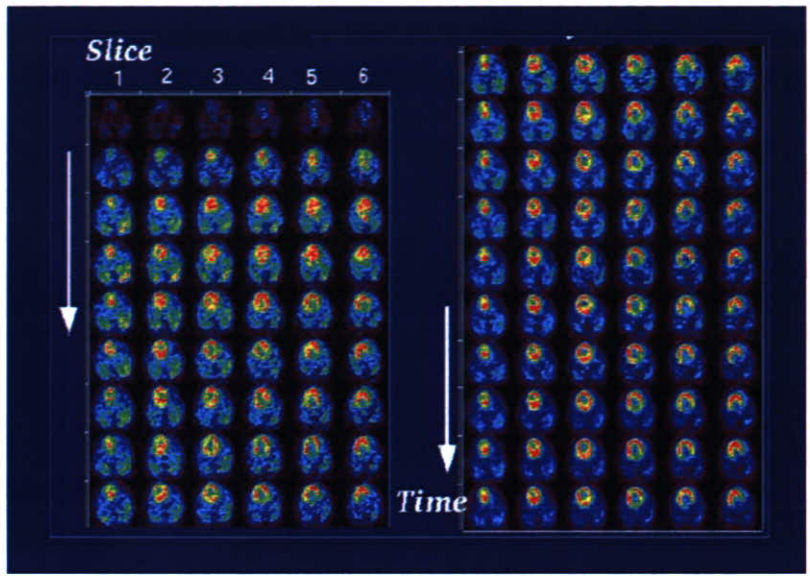

Fig. 4 A typical example of sequential SPECT images of the myocardium for six representative slices after intravenous injection of ^{201}Tl into a canine at rest

Fig. 3. The plasma to whole blood ratio curves could be approximated by the following equation:

$$R_{\mathrm{pl/wb}} = A_0 e^{-\lambda(t+\Delta t)^2} + A_1\left(1 - e^{-\lambda_2(t+\Delta t)}\right), \quad (3)$$

which resulted in A_0=1.303±0.045, A_1=0.7649±0.0056, λ_1=0.03636±0.0039 min^{-1}, λ_2=0.1263±0.0077 min^{-1} and Δt=0.9516±0.41 min. The correlation coefficient for the fit was r=0.995.

Figure 4 shows a typical example of sequential images after the intravenous injection of ^{201}Tl for six representative slices of a dog studied at rest. It can be seen that ^{201}Tl appeared in the ventricular chambers first and then gradually accumulated homogeneously into the left myocardium. The quality of these images is reasonably good, indicating that our approach of estimating the kinetic parameters by NLLSF is feasible without excessive noise

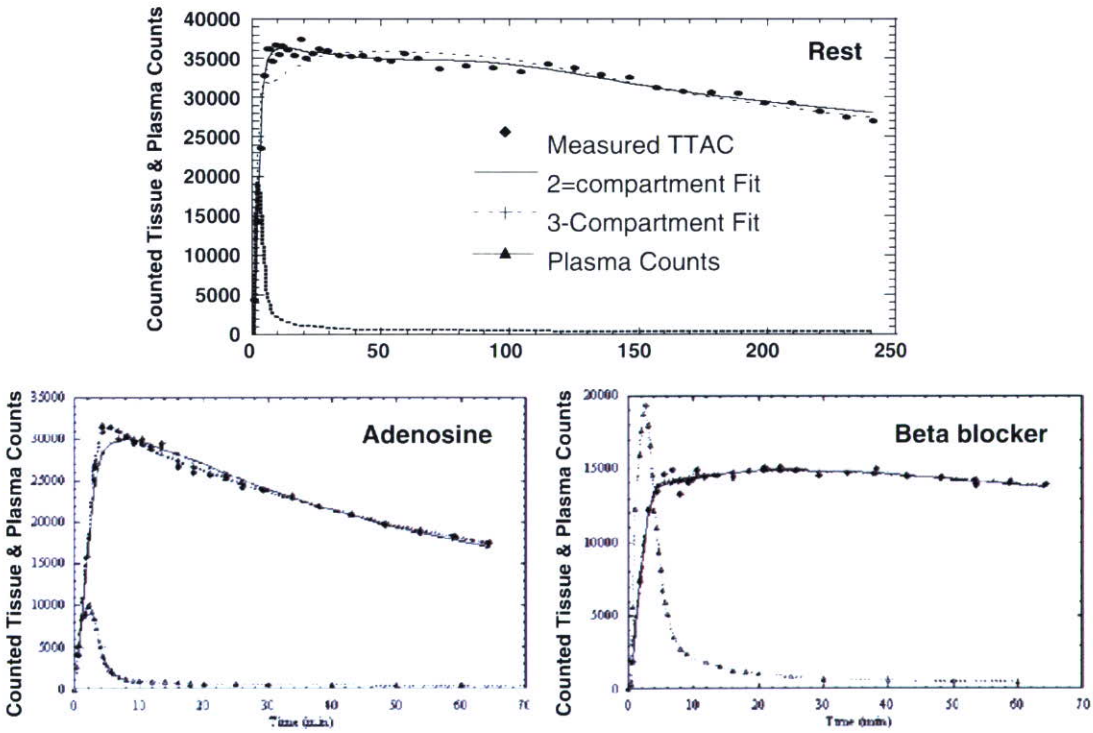

Fig. 5 TTACs and two- and three-compartment model fits for a resting, adenosine (increased MBF) and beta-blocker (reduced MBF) study. Note the different time scales for the resting study because resting studies were collected for 4 h compared to ≈1 h for the pharmacological intervention studies

amplification. Curve fits to representative TTACs for resting, beta-blocker and adenosine infusion studies are shown in Fig. 5. The height of the TTACs relative to the input function corresponded well with the pharmacological challenges. Compared to the resting studies, peaks of TTACs relative to the arterial input function were higher for adenosine and lower after beta-blocker administration. Results of kinetic fitting by the two- and three-compartment models are also plotted on this figure. Visually, the three-compartment model provided better fits than the two-compartment model to the observed TTACs, which is particularly evident for the initial scan period of the resting and adenosine studies.

Shown in Fig. 6a–e is the comparisons of K_1 obtained by NLLSF (three-compartment model fit) with the microsphere flow estimates. Values were averaged over the myocardial segments in both axes, thus each point corresponds to a single study. There was good correlation between K_1 and the microsphere flow when no corrections were applied, but K_1 significantly under-estimated the true flow (Fig. 6a). All the corrections improved the K_1 estimates (Fig. 6b–d) and the best agreement between K_1 and microsphere flow was observed when all three factors were corrected as described in Eq. 1 (Fig. 6e). Results of the regression analysis also demonstrated the highest correlation coefficient when all three correction factors were applied. Table 1 summarises the results of the Akaike information criteria (AIC) and Schwartz criteria (SC) obtained from the kinetic fitting analysis for all myocardial segments of all subjects. Both

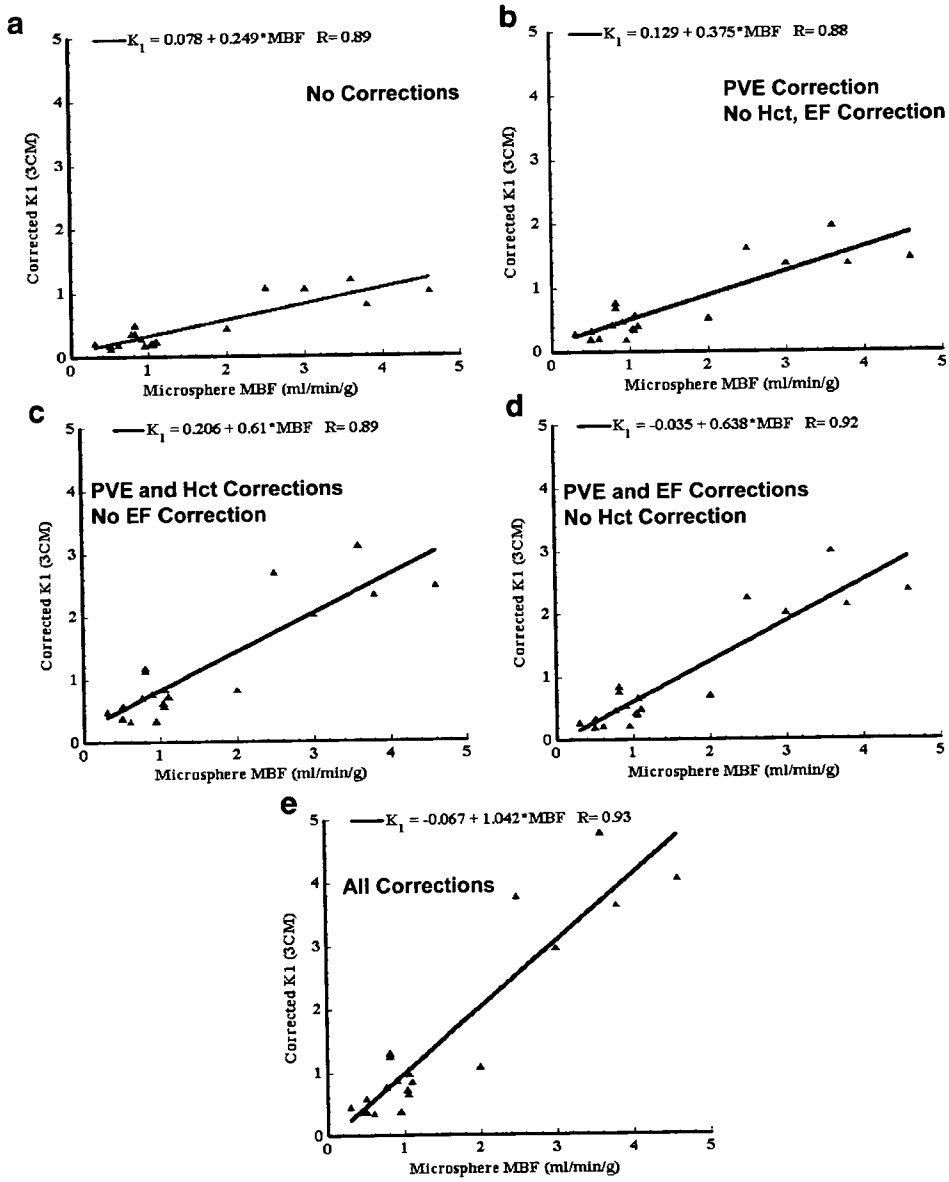

Fig. 6 Plot of K_1 derived from the three-compartment model fit against the mean of the pre- and post-dynamic SPECT microsphere blood flow measurements. **a** No correction for PVE, limited first-pass EF or conversion from plasma to blood flow has been applied. **b** Correction for PVE has been applied, but not for Hct or limited first-pass EF. **c** Corrections for PVE and Hct have been applied, but not for limited first-pass EF. **d** Corrections for PVE and limited first-pass EF have been applied, but not for Hct. **e** All corrections are applied for PVE, limited first-pass EF and Hct

Table 1 Summary of improvement in fit with the three-compartment model over the two-compartment model

Study group	Number of curves	Mean AIC two-compartment	Mean AIC three-compartment	Mean SC two-compartment	Mean SC three-compartment	Number of curves (%) (three-compartment better than two-compartment)[a]
Resting	35	652.4	630.2 ($p<0.01$)	663.8	638.4 ($p<0.01$)	24 (69)
Beta-blocker	20	378.4	378.8 (p=n.s.)	382.0 ($p<0.01$)	384.7	3 (15)
Adenosine	45	405.1	393.6 ($p<0.01$)	408.7	399.5 ($p<0.01$)	28 (62)

The p value indicates that the value in the cell is significantly lower than the corresponding other value.
AIC: Akaike information criterion, *SC*: Schwarz criterion
[a] This column gives the number of TTAC fits where the three-compartment model fit provided a significant improvement over the two-compartment fit according to all criteria (AIC, SC).

AIC and SC demonstrated that the three-compartment model fit provided significant improvement over the two-compartment model fit for resting and adenosine studies. For the beta-blocker studies, AIC between the two model fits was not significantly different, whilst SC demonstrated significantly better fit with the two-compartment model. Improved AIC and SC for the three-compartment model fit were observed in 69% of resting TTACs and 62% of adenosine TTACs, but only 15% in beta-blocker TTACs.

As shown in Fig. 7a and b, the K_1 and V_d values derived from the two-compartment model fit showed significant differences compared with those by the three-compartment model. Both K_1 and V_d were under-estimated with the two-compartment model fit compared with the three-compartment model fit. It should, however, be noted that there was a good correlation between the two- and three-compartment models for K_1, thus the bias introduced by the two-compartment model fit can potentially be corrected. K_1 values by the three-compartment model fit with all three corrections were 0.86±0.36, 2.71±1.64 and 0.55±0.24 ml/min/g corresponding to rest, adenosine infusion (with constant infusion at 140–700 mg/kg/h) and beta-blocker (with 2–6 mg administration), respectively. Difference in V_d was less than 10% and again this bias can potentially be corrected by the regression equation. The K_1 obtained with the two-compartment model also demonstrated a good correlation with the microsphere flow (Fig. 7c), though there was again a systematic under-estimation in K_1.

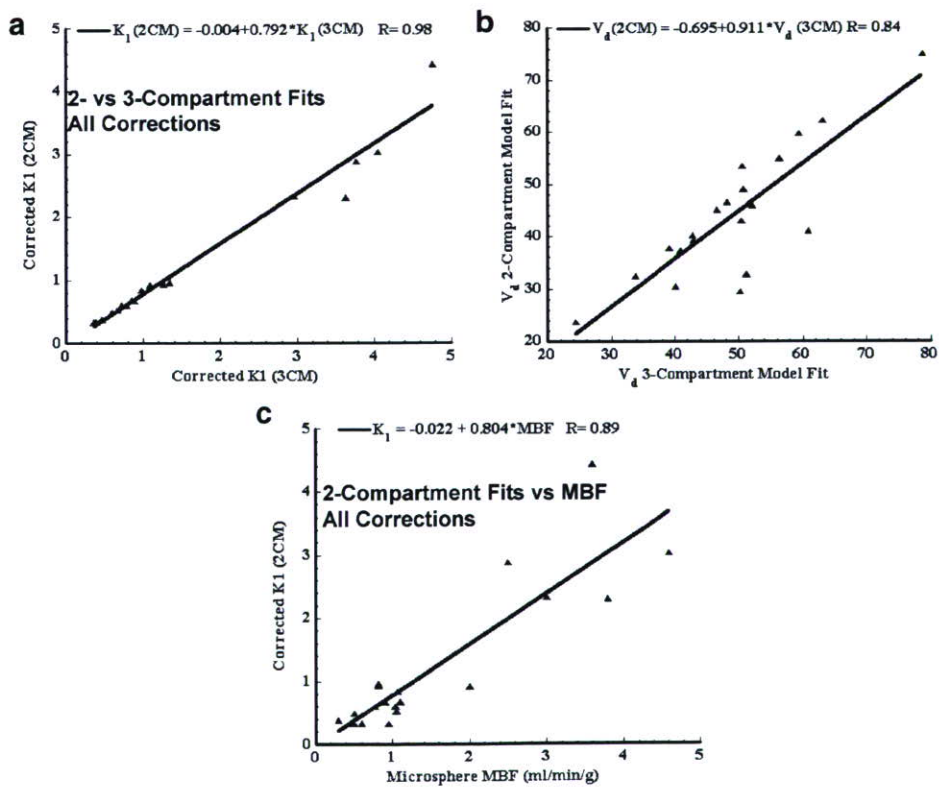

Fig. 7 **a** Plot of K_1 estimates derived from the two-compartment model fit against those from the three-compartment model fit. **b** Plot of V_d estimates derived from the two-compartment model fit against those from the three-compartment model fit. **c** Plot of K_1 values derived from the two-compartment model fit against mean of the pre- and post-dynamic SPECT microsphere blood flow measurements

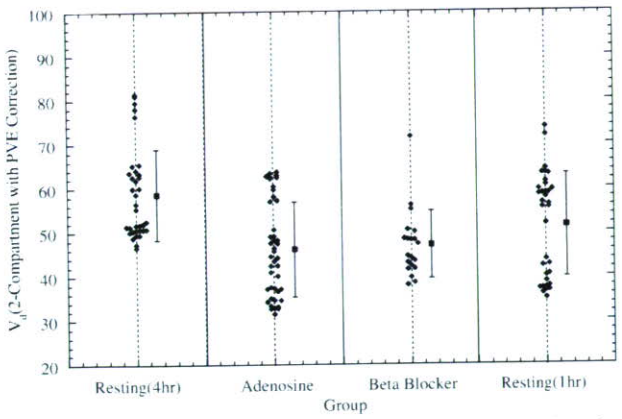

Fig. 8 V_d values obtained from the two-compartment model fit to the full 4 h resting data, adenosine and beta-blocker infusion 1 h curves and fit to first 1 h only of the resting study curves. Data from the multiple individual myocardial regions are shown

Figure 8 plots the V_d values for all evaluated myocardial segments for the fit to 4 h resting data, adenosine and beta-blocker infusion 1 h data and fit to only the first 1 h of resting data. The 4-h resting V_d values are significantly higher ($p<0.01$) compared with the adenosine, beta-blocker values and compared with the fit to the first 1 h resting data. However, the 1-h resting values are not significantly different from the beta-blocker V_d values nor the adenosine values.

Discussion

This study demonstrates that the kinetic analysis of quantitatively assessed myocardial ^{201}Tl accumulation (build-up and washout in healthy canines) provided quantitative MBF values, which agreed well with flows obtained using microspheres for a wide physiological range of flows. The size of the TTACs relative to the arterial plasma concentration corresponded well to the pharmacological stresses induced by adenosine and beta-blocker challenges. The compartmental model approach could reproduce these TTACs to make the determination of kinetic parameters, such as K_1 and V_d, possible. The three-compartment model gave results which were generally higher than the two-compartment model and which were statistically significantly better in terms of AIC, SC for the resting and adenosine studies, and this was in line with the visual inspection of the TTAC model fit curves. It should, however, be noted that the differences were only small between the two- and three-compartment model approaches, approximately 20% for K_1 and 10% for V_d The bias associated with the two-compartment model could be corrected by a linear regression as shown in Fig. 7a–c. This opens the possibility of using the more reliable two-compartment model fit due to its reduced number of parameters for routine clinical studies. The improved reliability of the two-compartment model fit in the clinical setting is particularly important if one intends to shorten the study time or generate parametric images.

The three corrections for PVE, Hct and first-pass EF proved to be important. The PVE correction method used in this work cannot, however, be applied to clinical studies, and the PVE correction in the beating heart still remains a considerable challenge in clinical studies. PVE may be reduced by gating the data, which may not, however, be feasible for the already noisy and large dynamic SPECT data sets. PVE may also be reduced by including resolution recovery as part of the reconstruction process [17–20]. Alternatively, it may also be possible to include PVE as part of the kinetic model fitting [21–25]. However, this adds extra fitting parameters and requires some parameters to be assumed fixed.

The input function is an important component in compartment model fitting. In this study, rapid arterial blood sampling was performed, and the plasma was separated by centrifugation. A number of important insights were gained by performing rapid separation of plasma in a subset of samples and dogs. It was found that ^{201}Tl enters the red blood cells as observed from the rapid separation of plasma in a subset of samples and dogs, which is not un-expected as potassium is also known [22] to be taken up by the red blood cells. The exchange of ^{201}Tl between red blood cells and plasma is relatively slow compared to the passage of blood through the capillary bed and hence direct uptake of activity from the red blood cells into tissue is believed to be negligible. Hence, tissue uptake will be dominated by the activity in the plasma during passage through the capillary bed and plasma in the substrate being measured. As a consequence, the flow measurement obtained with ^{201}Tl is plasma flow, which is in contrast to the microsphere studies, which measure whole blood flow. Conversion of plasma to blood flow was achieved by dividing the plasma flow by (1−Hct), as shown in Eq. 1, which then allowed the direct comparison with the microsphere measurements.

Rigorous estimation of the input function requires frequent arterial blood sampling. This is not only considered invasive, but also labor intensive. In addition, it has been shown in this study that rapid separation of the plasma for at least the first 30–40 min post-^{201}Tl administration is required to obtain accurate plasma concentration. If the separation of plasma is delayed, then the true plasma concentration at the time of sampling cannot be measured, which results in biased K_1 estimates. An empirical relationship of plasma to whole blood ratio as a function of time was developed and was found to be sufficiently consistent between dogs (Fig. 3) to allow the mean curve to be applied with minimal bias. Thus, in clinical practice, whole blood samples may be counted and converted to plasma concentration using the empirical relationship. This also potentially allows the input function to be obtained

non-invasively from the SPECT data using, for example, a curve derived from a left ventricular region. However, it should be noted that the relationship between plasma and whole blood counts in this study was derived for a 4-min infusion protocol and may be different for other injection protocols, such as bolus injection. Previously, it has been shown that population-based input functions calibrated with one or two blood samples could avoid the need for frequent arterial blood samples [26–28]. There is also a potential for applying this approach to ^{201}Tl studies. This is beyond the scope of this study and a systematic study should be designed to confirm this in clinical settings.

^{201}Tl has a high trans-capillary EF and thus the initial regional uptake of this tracer predominantly reflects the regional blood flow [10]. Use of a tracer that has a high first-pass EF is essential when one intends to quantitatively assess MBF at a high flow range or the coronary flow reserve. The EF of ^{201}Tl is reported as >0.8 [10] for a wide flow range and is known to be higher than ^{99m}Tc-labelled tracers such as tetrofosmine and sestamibi [29]. The physical characteristics of ^{201}Tl are unfortunately not ideal as low energy emission increases the attenuation factor and the scatter in the image. In addition, the relatively long half-life limits the administered activity to about a tenth of that with ^{99m}Tc tracers. Despite these shortcomings, the physiological characteristics of having high first-pass EF make ^{201}Tl an interesting tracer particularly for the absolute quantitation of MBF and the coronary flow reserve. This study demonstrates that quantitative physiological parameters can be derived from dynamic ^{201}Tl SPECT studies, despite its less than ideal imaging characteristics.

Whilst the quantitative physiological parameter estimation removed the systematic bias between MBF estimated by ^{201}Tl dynamic SPECT and by microspheres, the spread of data points around the regression line was rather large (Figs. 6e and 7c). This is not only due to possible errors in the estimation of MBF from the ^{201}Tl, but there was also considerable variation in flow estimated by the microspheres at the beginning and end of the study. Thus, at least part of the variability is attributable to errors in microsphere flow measurement, and particularly for the pharmaceutical intervention studies, flow may not have remained constant throughout the entire study duration, which may also account for some of the differences seen between the various flow measurements.

V_d estimated in this study could serve as an index of viability, as viable myocytes are required to maintain the large concentration gradient between plasma and myocardium at equilibrium. There was no significant difference in V_d values between rest, beta-blocker and adenosine studies when fitted for 1 h (Fig. 8). The significant difference between the 1- and 4-h fit for resting data could be explained by the limitation of the two-compartment model. Considerable spread in the V_d values observed over all dog studies on the other hand was partially attributed to the short (insufficient) scan time for reliable estimates of V_d. With the exception of the large, outlying V_d values in all 5 regions of 1 dog, the resting V_d values fell within a relatively narrow range of 47 to 65 (mean±SD=55±6). Given the sufficiently long scan time, significant reduction in V_d in infarcted areas may be detected. However, this would need to be tested with a suitable study design.

The scan time of 4 h required to achieve reliable V_d estimates is not practical in the routine clinical setting. As has been shown by Lau et al. [30], the scan period may be split into two sessions, an early dynamic scan for 30 min followed by a single static scan at approximately 3 h. This scheme is not more onerous than current rest/re-distribution protocols and hence could be practical. In addition, it may be possible to simplify the scanning protocol further to two static scans by using the table look-up method for the two-compartment model, which has been successfully employed for other SPECT tracers with relatively slow kinetics similar to ^{201}Tl [27, 31, 32]. This warrants further investigation.

This study relies on established, rigorous attenuation and scatter correction in SPECT [5] and availability of multi-detector SPECT systems capable of performing dynamic acquisition. To our knowledge, this is the first report that has demonstrated that it is possible to obtain quantitative physiological parameter estimates of K_1 and V_d in the myocardium using a clinical SPECT scanner and ^{201}Tl. This work suggests that it is feasible to apply our technique to clinical studies. Further studies are, however, needed to validate the proposed approach in the clinical setting. Incomplete motion correction is one possible error source, particularly in patients. Dynamic SPECT is probably more sensitive to the possible movement of patients during the study. Shortened clinical protocol is preferred, but this requires additional development to improve the reliability of parameter estimates. In addition, two scanning sessions are needed to assess the coronary flow reserve. We have recently demonstrated a technique to assess two cerebral blood flow images, one at rest and another after a vasodilating drug, from a single session of a SPECT scan in conjunction with split dose administration of ^{123}I-iodoamphetamine and dynamic SPECT [7]. As a clinical implication, the quantitative assessment of MBF and coronary flow reserve is important. For instance, coronary micro-vascular dysfunction or impaired endothelial function in patients with coronary risk factors or patients with cardiomyopathy or with heart failure is an un-resolved important issue to answer [11]. Coronary flow reserve can be reduced in patients with hypercholesterolemia without overt coronary stenosis [12]. A systematic study should be carried out to validate this approach for assessing MBF at rest and after adenosine from a single session of a scan.

Acknowledgement This study was supported by the Budget for Nuclear Research of the Ministry of Education, Culture, Sports, and Technology (MEXT), Japan; a grant from the Cooperative Link of Unique Science and Technology for Economy Revitalization promoted by the Ministry of Education, Culture, Sports and Technology, Japan and a grant for translational research from the Ministry of Health, Labour and Welfare (MHLW), Japan. We would like to thank Nihon Medi-Physics, Hyogo, Japan for providing the ^{201}Tl samples and also Mr. Yoshihide Takatani for his invaluable suggestion on the study design.

References

1. Gullberg GT, Huesman RH, Ross SG, et al. Dynamic cardiac single-photon emission computed tomography. In: Beller GA, Zaret BL, editors. Nuclear cardiology: state of the art and future directions. Philadelphia, PA: Mosby-Year Book Inc.; 1998. p. 137–87.
2. Chiao PC, Ficaro EP, Dayanikli F, Rogers WL, Schwaiger M. Compartmental analysis of technetium-99m-teboroxime kinetics employing fast dynamic SPECT at rest and stress. J Nucl Med 1994;35(8):1265–73.
3. Narita Y, Eberl S, Iida H, Hutton BF, Braun M, Nakamura T, et al. Monte Carlo and experimental evaluation of accuracy and noise properties of two scatter correction methods for SPECT. Phys Med Biol 1996;41(11):2481–96.
4. Narita Y, Iida H, Eberl S, Nakamura T. Monte Carlo evaluation of accuracy and noise properties of two scatter correction methods for ^{201}Tl cardiac SPECT. IEEE Trans Nucl Sci 1997;44:2465–72.
5. Iida H, Shoji Y, Sugawara S, Kinoshita T, Tamura Y, Narita Y, et al. Design and experimental validation of a quantitative myocardial ^{201}Tl SPECT System. IEEE Trans Nucl Sci 1999;46:720–6.
6. Iida H, Narita Y, Kado H, Kashikura A, Sugawara S, Shoji Y, et al. Effects of scatter and attenuation correction on quantitative assessment of regional cerebral blood flow with SPECT. J Nucl Med 1998;39(1):181–9.
7. Kim KM, Watabe H, Hayashi T, Hayashida K, Katafuchi T, Enomoto N, et al. Quantitative mapping of basal and vasareactive cerebral blood flow using split-dose ^{123}I-iodoamphetamine and single photon emission computed tomography. Neuroimage 2006;33(4):1126–35.
8. Beller GA, Watson DD, Pohost GM. Kinetics of thallium distribution and redistribution: clinical applications in sequential myocardial imaging. In: Pitt B, Strauss HW, editors. Cardiovascular nuclear medicine. St. Louis: Mosby; 1979. p 225–42.
9. Berman DS, Maddhi J, Garcia EV. Role of thallium-201 imaging in the diagnosis of myocardial ischemia and infarction. In: F HS, editor. Nuclear medicine annual. New York: Raven; 1980. p 1–55.
10. Weich HF, Strauss HW, Pitt B. The extraction of thallium-201 by the myocardium. Circulation 1977;56(2):188–91.
11. Camici PG, Crea F. Coronary microvascular dysfunction. N Engl J Med 2007;356(8):830–40.
12. Yokoyama I, Ohtake T, Momomura S, Nishikawa J, Sasaki Y, Omata M. Reduced coronary flow reserve in hypercholesterolemic patients without overt coronary stenosis. Circulation 1996;94 (12):3232–8.
13. Li J, Tsuji BMW, Welch A, Frey EC, Gullberg GT. Energy window optimization in simultaneous Technetium-99m and Thallium-201 SPECT data acquisition. IEEE Trans Nucl Sci 1995;42:1207–13.
14. Meikle SR, Hutton BF, Bailey DL. A transmission-dependent method for scatter correction in SPECT. J Nucl Med 1994;35(2):360–7.
15. Hudson HM, Larkin RS. Accelerated image reconstruction using srdered subsets of projection data. IEEE Trans Med Imag 1994;13:601–9.
16. Choi Y, Hawkins RA, Huang SC, Brunken RC, Hoh CK, Messa C, et al. Evaluation of the effect of glucose ingestion and kinetic model configurations of FDG in the normal liver. J Nucl Med 1994;35(5):818–23.
17. Hutton BF, Hudson HM, Beekman FJ. A clinical perspective of accelerated statistical reconstruction. Eur J Nucl Med 1997;24 (7):797–808.
18. Hutton BF, Lau YH. Application of distance-dependent resolution compensation and post-reconstruction filtering for myocardial SPECT. Phys Med Biol 1998;43(6):1679–93.
19. Pretorius PH, King MA, Pan TS, de Vries DJ, Glick SJ, Byrne CL. Reducing the influence of the partial volume effect on SPECT activity quantitation with 3D modelling of spatial resolution in iterative reconstruction. Phys Med Biol 1998;43(2): 407–20.
20. Soares EJ, Glick SJ, King MA. Noise chaeacterization of combined Bellini-type attenuation correction and frequency-distance principle restoration filtering SPECT. IEEE Trans Nucl Sci 1996;43:3278–90.
21. Iida H, Kanno I, Takahashi A, Miura S, Murakami M, Takahashi K, et al. Measurement of absolute myocardial blood flow with H215O and dynamic positron-emission tomography. Strategy for quantification in relation to the partial-volume effect. Circulation 1988;78(1):104–15.
22. Araujo LI, Lammertsma AA, Rhodes CG, McFalls EO, Iida H, Rechavia E, et al. Noninvasive quantification of regional myocardial blood flow in coronary artery disease with oxygen-15-labeled carbon dioxide inhalation and positron emission tomography. Circulation 1991;83(3):875–85.
23. Bergmann SR, Herrero P, Markham J, Weinheimer CJ, Walsh MN. Noninvasive quantitation of myocardial blood flow in human subjects with oxygen-15-labeled water and positron emission tomography. J Am Coll Cardiol 1989;14(3):639–52.
24. Iida H, Rhodes CG, de Silva R, Yamamoto Y, Araujo LI, Maseri A, et al. Myocardial tissue fraction-correction for partial volume effects and measure of tissue viability. J Nucl Med 1991;32(11): 2169–75.
25. Iida H, Tamura Y, Kitamura K, Bloomfield PM, Eberl S, Ono Y. Histochemical correlates of (15)O-water-perfusable tissue fraction in experimental canine studies of old myocardial infarction. J Nucl Med 2000;41(10):1737–45.
26. Iida H, Itoh H, Nakazawa M, Hatazawa J, Nishimura H, Onishi Y, et al. Quantitative mapping of regional cerebral blood flow using iodine-123-IMP and SPECT. J Nucl Med 1994;35(12):2019–30.
27. Onishi Y, Yonekura Y, Nishizawa S, Tanaka F, Okazawa H, Ishizu K, et al. Noninvasive quantification of iodine-123-iomazenil SPECT. J Nucl Med 1996;37(2):374–8.
28. Takikawa S, Dhawan V, Spetsieris P, Robeson W, Chaly T, Dahl R, et al. Noninvasive quantitative fluorodeoxyglucose PET studies with an estimated input function derived from a population-based arterial blood curve. Radiology 1993;188(1):131–6.
29. Fukushima K, Momose M, Kondo C, Kusakabe K, Kasanuki H. Myocardial kinetics of (201)Thallium, (99m)Tc-tetrofosmin, and (99m)Tc-sestamibi in an acute ischemia-reperfusion model using isolated rat heart. Ann Nucl Med 2007;21(5):267–73.
30. Lau CH, Eberl S, Feng D, Iida H, Lun PK, Siu WC, et al. Optimized acquisition time and image sampling for dynamic SPECT of Tl-201. IEEE Trans Med Imag 1998;17(3): 334–43.
31. Iida H, Itoh H, Bloomfield PM, Munaka M, Higano S, Murakami M, et al. A method to quantitate cerebral blood flow using a rotating gamma camera and iodine-123 iodoamphetamine with one blood sampling. Eur J Nucl Med 1994;21(10):1072–84.
32. Onishi Y, Yonekura Y, Mukai T, Nishizawa S, Tanaka F, Okazawa H, et al. Simple quantification of benzodiazepine receptor binding and ligand transport using iodine-123-iomazenil and two SPECT scans. J Nucl Med 1995;36(7):1201–10.

Ann Nucl Med (2008) 22:1–11
DOI 10.1007/s12149-007-0083-2

REVIEW ARTICLE

PET kinetic analysis: error consideration of quantitative analysis in dynamic studies

Yoko Ikoma · Hiroshi Watabe · Miho Shidahara
Mika Naganawa · Yuichi Kimura

Received: 8 June 2007 / Accepted: 3 October 2007

Abstract Positron emission tomography dynamic studies have been performed to quantify several biomedical functions. In a quantitative analysis of these studies, kinetic parameters were estimated by mathematical methods, such as a nonlinear least-squares algorithm with compartmental model and graphical analysis. In this estimation, the uncertainty in the estimated kinetic parameters depends on the signal-to-noise ratio and quantitative analysis method. This review describes the reliability of parameter estimates for various analysis methods in reversible and irreversible models.

Keywords PET · Compartmental model · Error analysis

Introduction

Quantification of in vivo tracer studies has been performed with positron emission tomography (PET) to assess biomedical functions, such as cerebral blood flow [1], cerebral metabolic rate of glucose [2], and neuroreceptor binding [3]. In those studies, PET data were acquired sequentially, and kinetic parameters that describe the behavior of the administered radiopharmaceutical in tissue were estimated by using a mathematical model from the time–activity curve (TAC) of each tissue or voxel [4]. This model is assumed to take into account the chemical and pharmacological properties of the tracer, physical properties of the measurement system, stability of the mathematical solution, and so on.

Positron emission tomography data include the noise originating from a variety of factors such as the kinetics of the tracer, injection dosage, scan protocol, and sensitivity of the PET camera. In quantitative analysis, the uncertainty in estimated kinetic parameters is affected by this noise. Moreover, the effect of noise depends on the analysis method employed, such as the number of model parameters, estimation algorithm, size of regions of interest (ROIs) and voxels. Therefore, a stable model is necessary, in addition to reducing the noise of the original image, for reliable estimation of the kinetic parameters. A basic quantification method is based on a nonlinear least-squares (NLS) fitting with a compartmental model [4], and several methods have been proposed for stable and rapid estimation. A simplified method such as graphical analysis or reference tissue methods produces an improvement in the reliability of parameter estimates; however, in some cases it brings about a lack of information or causes bias (underestimation or overestimation) regarding the kinetic parameters. Each analysis method has its own properties, and it is important to know the properties of each method for the assessment of biomedical functions with high precision.

In this review, we discuss the reliability of estimated parameters by several approaches, such as analysis methods in a reversible model with and without arterial input function, and analysis methods in irreversible model.

Y. Ikoma (✉) · H. Watabe
Department of Investigative Radiology, National Cardiovascular Center Research Institute, 5-7-1 Fujishiro-dai, Suita 565-8565, Japan
e-mail: ikoma@ri.ncvc.go.jp

M. Shidahara · M. Naganawa · Y. Kimura
Molecular Imaging Center, National Institute of Radiological Sciences, Chiba, Japan

M. Naganawa
Japan Society for the Promotion of Science, Tokyo, Japan

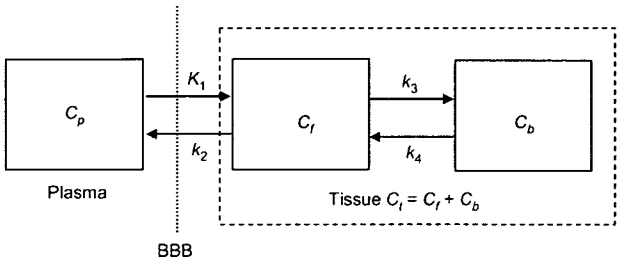

Fig. 1 Reversible two-tissue compartment model. BBB represents the blood–brain barrier, C_p represents the compartment of plasma, C_f represents free and nonspecific binding in tissue, and C_b represents specific binding. K_1–k_4 are rate constants between two compartments. Total radioactivity in the tissue enclosed with a rectangular of a *broken line* is expressed as a sum of C_f and C_b

Parameter estimation in a reversible model with arterial input function

A reversible two-tissue compartment model (Fig. 1) is often used for the quantification of the total distribution volume ($V_T = K_1/k_2(1 + k_3/k_4)$) or binding potential (BP = k_3/k_4) in neuroreceptor or transporter studies [3, 5]. Here, "reversible" means that the tracer reversibly binds to the neuroreceptor or transporter. The analysis methods of these studies are divided into two general groups, namely, a compartmental model-based method and a noncompartmental model method such as graphical analysis. These two methods differ in the property of uncertainty regarding parameter estimates. Moreover, the uncertainty depends on whether estimation is performed with arterial input function. The methods with arterial input function include errors in plasma TAC caused by measurement of plasma samples, metabolite correction, and delay correction between plasma and tissue, whereas the methods without arterial input function require constraints to eliminate the plasma input function. In this section, error evaluation of nonlinear or linear least-squares fitting with a reversible compartment model and graphical analysis with arterial input function are described.

Compartmental analysis

In a two-tissue compartment model, the radioactivity of the target region is expressed as a summation of two compartments in Eq. 1:

$$C_t(t) = \frac{K_1}{\alpha_1 - \alpha_2}\{(\alpha_1 - k_3 - k_4)e^{-\alpha_1 t} - (\alpha_2 - k_3 - k_4)e^{-\alpha_2 t}\} \otimes C_p(t) \quad (1)$$

$$\alpha_{12} = \frac{k_2 + k_3 + k_4 \pm \sqrt{(k_2 + k_3 + k_4)^2 - 4k_2k_4}}{2}$$

where C_p and C_t are the radioactivity concentrations in plasma and target tissue with specific binding, respectively; K_1 to k_4 are rate constants between the two compartments, and $\otimes$ is a mathematical operator of convolution. This equation is nonlinear in each parameter because no linear relation can be found between the parameters and be found in a sum of squared differences between a predicted and measured PET data. Therefore, the fitting procedure is iterative [6], and the parameters vary from the given initial values using an optimization algorithm, such as the Newton–Gaussian or Levenberg–Marquart algorithms [7, 8], until the residual sum of squares (RSS) or weighted RSS reaches its minimum.

In this NLS method, estimated parameters are markedly affected by the noise in PET data. Although they do not cause a bias at a low noise level, their coefficient of variation [COV; SD/mean (%)] becomes larger as noise increases, and COV is much larger than in graphical analysis. With some tracers, unconstrained NLS fit with a two-tissue compartment model shows K_1/k_2 changing with V_T, and BP might occasionally have no biological significance. To improve the reliability of BP estimates, fixed K_1/k_2 value derived from a reference region is often utilized for nonlinear fitting on the assumption that K_1/k_2 is common to whole regions [5]. However, in some tracers, the constraint on K_1/k_2 is difficult because a region without specific binding, such as the radioligand for the peripheral benzodiazepine receptors [^{11}C]DAA1106 [9], cannot be determined or because uptake is actively related to a function of blood–brain barrier such as [^{11}C]verapamil [10]. In some cases, a one-tissue compartment model is sufficient to describe the kinetics of the tracer [5], and COV of parameter estimates with the one-tissue compartment model is much smaller than that of a two-tissue compartment model [5, 11]. However, tracers whose arrival in equilibrium is slow cannot be described using the one-tissue compartment model.

The advantage of NLS with a two-tissue compartment model is that every parameter K_1 to k_3 can be estimated, and that it is free from the biases and assumptions that arise in linearization or simplification. The disadvantage is that COV is large, especially in voxel-by-voxel estimation, and that the fitting procedure is computationally very expensive. Therefore, this method is useful for ROI analysis, in which parameters are estimated in a mean TAC within an ROI, but it is not practical for parametric mapping with voxel-based estimation.

Meanwhile, linear least-squares (LLS) methods based on one- or two-tissue compartment models have been proposed [12, 13]. The LLS with a two-tissue compartment model is expressed as Eq. 2:

$$C_t(T) = P_1\int_0^T C_p(t)dt + P_2\int_0^T\int_0^s C_p(t)dtds + P_3\int_0^T C_t(t)dt + P_4\int_0^T\int_0^s C_t(t)dtds \quad (2)$$

where $P_1 = K_1$, $P_2 = K_1(k_3 + k_4)$, $P_3 = -(k_2 + k_3 + k_4)$, and $P_4 = -k_2k_4$.

The parameters of K_1 to k_4 are calculated by $K_1 = P_1$, $k_2 = -P_2/P_1 - P_3$, $k_3 = -P_3 - k_2 - k_4$, and $k_4 = -P_4/k_2$. This method allows estimation of P_1 to P_4 by linear regression analysis, which requires no iteration process, assuming that the integrals of plasma and tissue data are noise free. Therefore, the processing speed is fast, making it possible to obtain parametric mapping in a short time. However, estimated parameters are biased especially in a high noise level because the noise contained in Eq. 2 is not only the direct measurement noise of C_t on the left side of Eq. 2, but also the linear combinations of the integrations of these measurement errors on the right side. Moreover, the COV is large because four parameters are estimated through multilinear regression, with an equation consisting of four variable terms. Ichise et al. [13] compared this method with NLS and graphical analysis methods in simulations and actual PET data of the 5-HT_{1A} ligand [^{18}F]FCWAY and the 5-HT_{2A} ligand [^{11}C]MDL100907, and reported that the bias and COV of LLS method are larger than those of the NLS method.

Graphical analysis

The graphical analysis of Logan (LGA) yields the total distribution volume by arterial input function and tissue TAC from the equation:

$$\frac{\int_0^T C_t(t)dt}{C_t(T)} = V_t\frac{\int_0^T C_p(t)dt}{C_t(T)} + b \quad \text{for} \quad t > t^* \quad (3)$$

where C_p and C_t are the radioactivity concentrations in plasma and target tissue, respectively, and the parameter V_T is the corresponding total distribution volume, although, strictly speaking, it contains the blood volume [14, 15]. The relation holds only after equilibration time t^*, i.e., $dC_b/dt = 0$, where C_b is the radioactivity concentration in specific binding compartment, V_T and b are estimated as a slope and an intercept, respectively, by using data sets after t^*. This method is simple, stable, needs no assumption about the number of compartments, and the estimation process is rapid. Therefore, this is very useful for not only ROI-based analysis but also voxel-based parametric mapping. However, there are two drawbacks to this method, noise-induced bias caused by the statistical noise in $C_t(T)$ of the right side of Eq. 3 [16] and determination of t^*. The details of this method have been reviewed by Kimura et al. [15].

Several methods for reducing this noise-induced bias have been suggested. Logan et al. [17] applied the iterative method called generalized linear least squares developed by Feng et al. [12] to generate smoothed TACs, and reported that LGA with smoothed TACs reduced the noise-induced bias. Varga et al. [18] derived a slope and an intercept of Eq. 3 by minimizing the sum of squared perpendicular rather than the vertical y-axis distance between the data points and fitted straight line, stating that the bias of V_T estimates was small even though COV increased with the noise in simulated data of dopamine D_1 receptor ligand [^{11}C]NNC112 and dopamine transporter ligand [^{11}C]d-threo-methylphenidate and measured data of serotonin transporter ligand [^{11}C](+)McN5652 [18]. Another approach was rearranging the equation of LGA into multilinear form, and it was demonstrated that this multilinear analysis (MA) reduced noise-induced bias for both the one-tissue compartment model [19] and the two-tissue compartment model expressed as Eq. 4 [13]:

$$C_t(T) = -\frac{V_T}{b}\int_0^T C_p(t)dt + \frac{1}{b}\int_0^T C_t(t)dt \quad \text{for} \quad t > t^* \quad (4)$$

In Eq. 4, only the integral of $C_t(t)$ is included as a potential noise source in linear regression, and the integral of $C_t(t)$ reduces the noise in C_t of each frame. However, the COV of V_T is larger than LGA, especially in tracers with slow kinetics given that two parameters of Eq. 4: V_t/b and $1/b$ are estimated by multilinear regression, and not by a straight line like LGA [9, 13]. For tracers with early t^*, enough data points for linear regression can be obtained after equilibrium, making the MA method useful for a V_T estimation. However, this method is not appropriate for slow kinetics tracers, because too few points for linear regression cause a large COV derived from noise in the PET data. Meanwhile, Ogden et al. [20] were able to eliminate the noise-induced bias by likelihood estimation.

For these methods based on LGA, the determination of optimal t^* is burdensome because selection of earlier t^* before equilibrium causes underestimation of V_T because early points are not on the straight line expressed as Eq. 3, whereas estimates with late t^* are often affected by noise. Moreover, in some tracers such as 5-HT_{2A} receptor ligand [^{11}C]MDL100907, an equilibrium state cannot be reached during a PET scan [13]. Furthermore, the equilibrium time t^* may differ with regions or subjects if their kinetics are different. Automatic selection of t^* was proposed, in which if the maximal value of the absolute difference between observed and predicted

Table 1 Summary of typical reversible model with arterial input function

	NLS	LLS	LGA	MA
Estimated physiological parameter	K_1, k_2, k_3, k_4	K_1, k_2, k_3, k_4	V_T	V_T
Fitting range	0, End frame	0, End frame	$t > t^*$	$t > t^*$
Fitting algorithm	Nonlinear	Multilinear	Linear	Multilinear
Estimation speed	Slow	Fast	Fast	Fast
Estimation error	Bias is small COV is large	Bias is large in a high noise level COV is large	Bias is large COV is small	Noise-induced bias of LGA is eliminated COV is large in slow kinetics tracer

NLS nonlinear least squares with a two-tissue compartment model, *LLS* linear least squares with a two-tissue compartment model, *LGA* Logan graphical analysis, *MA* multilinear analysis, t^* equilibrium time

values within the fitting period is less than a prescribed value, then the starting point of the fitting period is taken as t^* [21]. However, the prescribed value of error should be chosen according to the noise level of the TAC. For example, for ROI-based analysis of [^{18}F]FCWAY, prescribed values of 10% and 20% are appropriate in the frontal cortex and raphe, respectively [13].

Another disadvantage of these methods based on LGA is that the estimated parameter is only V_T. V_T is a complex parameter of K_1/k_2 and BP. In general, BP and V_T are considered to be parallel to each other on the assumption that there are small variations of K_1/k_2 among regions or individuals. If K_1/k_2 varies markedly among individuals or comparison groups, V_T must be carefully interpreted.

Models described in this section are summarized in Table 1.

Error evaluation in estimates for [^{11}C]FLB 457 studies

In this section, we demonstrate properties of the errors of parameters by the various methods introduced in the above section. Estimated reliabilities of NLS, LGA, and MA methods in [^{11}C]FLB 457 simulation studies are shown in Figs. 2, 3, and 4. In this simulation study, TACs of [^{11}C]FLB 457 for the temporal cortex were computed using a measured arterial input function and a given true parameter value [$K_1 = 0.39$ (ml g^{-1} min^{-1}), $k_2 = 0.09$ (min^{-1}), $k_3 = 0.035$ (min^{-1}), $k_4 = 0.04$ (min^{-1})] [22] with Eq. 1, and Gaussian noise was added with variance proportional to the true count of each frame taking into account the physical decay and frame duration (Fig. 2). This simulation assumes that the noise is determined by the count of the curve itself. In fact, the noise is determined by the total count of the slice [23], and is affected by scatter, random, dead time, and so on. The level of the noise for the dynamic data in this simulation was expressed as the mean of SD between the frames from 1 to 90 min. One thousand TACs were realized for each

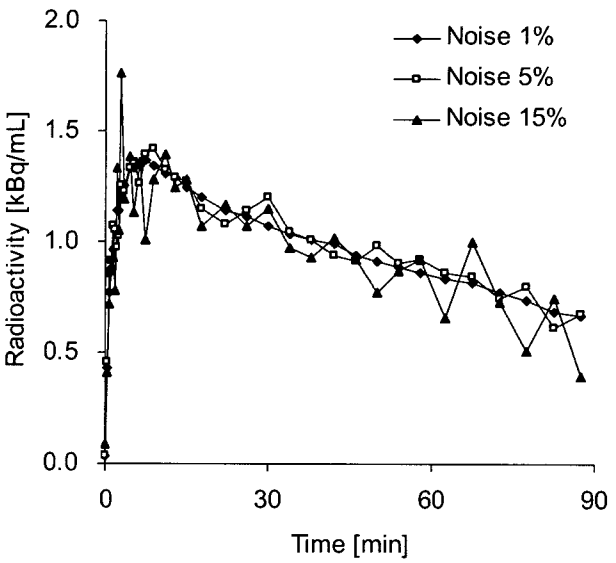

Fig. 2 Simulated time–activity curves for [^{11}C]FLB 457 at noise levels of 1%, 5%, and 15%, respectively

noise level of 1%, 3%, 5%, 7%, 10%, and 15%, V_T was estimated for each TAC by NLS, LGA, and MA, and the mean and SD of 1000 estimates were calculated. In LGA and MA, start time for linear regression t^* was set at 30 min. V_T estimates were considered invalid if $V_T < 0$ or more than twice the true value.

Figure 3 shows the relationship between the noise level and reliability of V_T estimates. Underestimation of V_T was observed in LGA when the noise level was 5%, and became larger with increasing noise (Fig. 3a). Deducing from the TAC of [^{11}C]FLB 457 human data, the noise level of ROI-based estimation is under 3%, and that of voxel-based estimation is about 15% or more. Therefore, this bias is problematic in voxel-based estimation. Meanwhile, there is little bias in MA. In NLS, there was no bias at a low noise level. The COV was smallest in LGA, whereas that in NLS was much larger than in the other

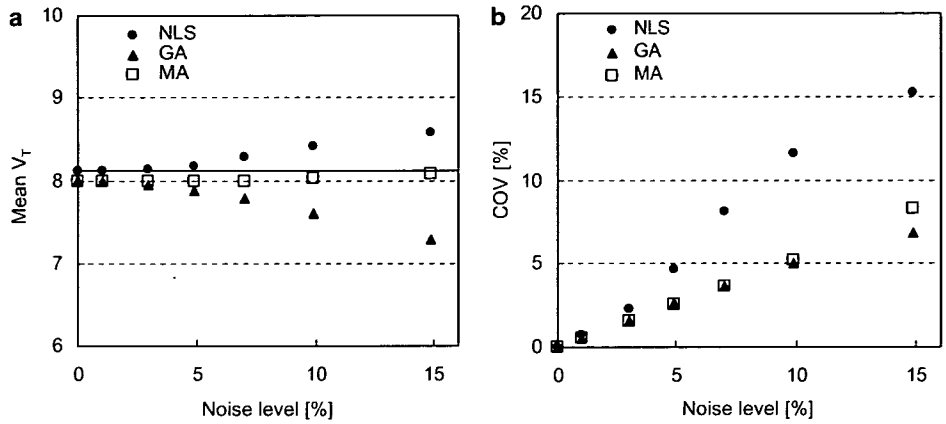

Fig. 3 Relationship between noise and reliability for the methods of nonlinear least squares, graphical analysis (GA), and multilinear analysis (MA), respectively. The mean value (**a**) and coefficient of variation (**b**) of V_T estimates for simulation data with noise at 1%, 3%, 5%, 7%, 10%, and 15% are shown. V_T of GA and MA were estimated with start points t^* of 30 min. *Solid line* in (**a**) represents the true value of V_T

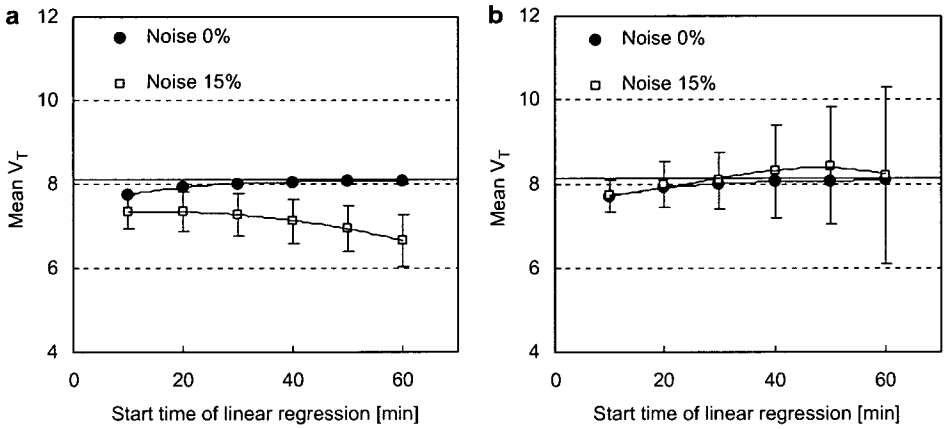

Fig. 4 Relationship between the start time of linear regression and V_T estimated with GA (**a**) and MA (**b**). Shown are estimated V_T for a simulation data without noise and the mean value and SD of V_T for a simulation data with 15% noise. *Solid lines* represent true values

methods (Fig. 3b). In MA, the COV was almost the same as that in LGA at a low noise level, becoming larger as the noise increased.

Next, the relationship between the start time of the linear regression and V_T estimates is shown in Fig. 4. Both the LGA and MA provided the true V_T in the case of noise-free TAC given when t^* was 30 min. However, in the TACs with 15% noise, V_T of LGA was underestimated when compared with that in TAC without noise because of the large noise, and it became worse in later t^* (Fig. 4a). Meanwhile, in MA, underestimation caused by noise was not observed; however, COV of V_T estimates was serious in later t^* owing to small data points for regression (Fig. 4b).

Parameter estimation in a reversible model without arterial input function

Reference tissue methods eliminate an arterial plasma TAC arithmetically from model equations by using a TAC of reference region where specific bindings are negligible, and these methods have been widely used to estimate neuroreceptor ligand binding because they do not require invasive arterial blood sampling. Several methods have been proposed for BP estimation with reference regions, and are divided into two groups. One approach is based on the compartmental model with reference tissue, such as a simplified reference tissue model [24], and the other is based on the graphical analysis method of Logan et al. [25]. In this section, the error properties of these methods are described.

Simplified reference tissue model

The radioactivity of the target and reference region is expressed in Eqs. 1 and 5, respectively, when a two-tissue compartment four-parameter model is assumed for the target region whereas a one-tissue compartment two-parameter model without specific binding compartment is assumed for the reference region (Fig. 5):

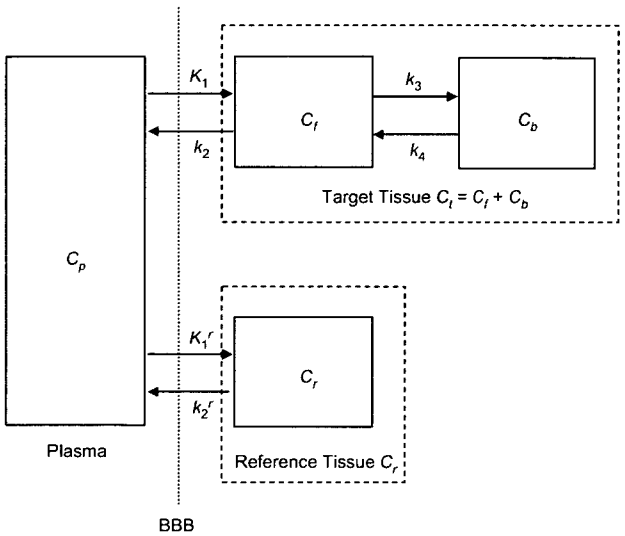

Fig. 5 Reference tissue model. Compartment C_r represents free plus nonspecific binding in reference tissue, and K_1^r and k_2^r describe the rate constants between plasma and reference tissue

$$C_t(T) = \frac{K_1}{\alpha_1 - \alpha_2}\{(\alpha_1 - k_3 - k_4)e^{-\alpha_1 t} - (\alpha_2 - k_3 - k_4)e^{-\alpha_2 t}\} \otimes C_p(t), \quad (1)$$

$$\alpha_{1,2} = \frac{k_2 + k_3 + k_4 \pm \sqrt{(k_2 + k_3 + k_4)^2 - 4k_2k_4}}{2}$$

$$C_r(t) = K_1^r e^{-k_2^r t} \otimes C_p(t) \quad (5)$$

where C_r is the radioactivity concentration in the reference tissue, and K_1^r and k_2^r are rate constants of the reference tissue.

The original approach of the reference tissue model was developed with the two-tissue compartment model for the target region [26, 27] by replacing C_p in Eq. 1 with Eq. 5 under the assumptions that K_1/k_2 of the target to reference was equal. Later, this method was evolved to the simplified reference tissue model (SRTM) by following the one-tissue compartment model in the target region [24]. This SRTM estimates three parameters by NLS: the delivery ratio of the target to the reference region ($R_1 = K_1/K_1^r$), the clearance rate constant of the target region (k_2), and BP as shown in Eq. 6:

$$C_t(t) = \theta_1 C_r(t) + \theta_2 C_r(t) \otimes e^{-\theta_3 t} \quad (6)$$

$$\begin{cases} \theta_1 = R_1 \\ \theta_2 = R_1 k_2^r \left(1 - \dfrac{R_1}{1+\mathrm{BP}}\right) = k_2 \left(1 - \dfrac{R_1}{1+\mathrm{BP}}\right) \\ \theta_3 = k_2/(1+\mathrm{BP}) \end{cases}$$

This method has been used widely in neuroreceptor studies. Not only BP but also R_1 can be estimated, and there is no bias owing to a linearization. However, in some cases with low binding, especially when $\theta_2 = 0$, SRTM was unable to find a solution even for a low noise level, because the parameter k_2 becomes numerically unidentifiable in this case [28]. Moreover, in a voxel-by-voxel estimation, the estimated parameters are affected by the noise in tissue TAC, and the computer time is lengthy because the nonlinear estimation is invoked. Therefore, this method is useful for ROI-based estimation but is not practical for voxel-based estimation.

Subsequently, to achieve rapid estimation for receptor mapping, a new method using basic functions (basis function method; BFM), including parameter boundaries, was developed [28]. The nonlinear term $C_r(t) \otimes \exp(-\theta_3 t)$ in Eq. 6 is computed for a discrete θ_3 value covering physiologically acceptable ranges prior to parameter estimation. For each value of θ_3, θ_1 and θ_2 can then be calculated by the linear least-squares technique, which is much faster than the nonlinear one. In the simulation study of Gunn et al. [28], there was essentially no difference between NLS and BFM in terms of bias or variance. However, when the noise level was high, NLS was unstable and gave an unreasonably large value for BP; these outliers are avoided with BFM because of the parameter boundaries introduced in the exponential term, i.e., θ_3. This method is often used for neuroreceptor mapping with voxel-by-voxel estimation. Note that the range of the θ_3 value must be selected to encompass all plausible values for θ_3 governed by k_2 and BP, and so this range needs to be set appropriately according to the tracer.

Meanwhile, a two-step method of SRTM (SRTM2) developed by Wu et al. [29] reduced noise in the parameter estimates for functional images by using a fixed value for the clearance rate constant of the reference region k_2^r, because the true value of k_2^r should not vary across brain voxels. In functional imaging with SRTM2, the three parameters of SRTM are estimated and k_2^r is calculated from $\theta_2 = \theta_1 k_2^r - \theta_1\theta_3$ of Eq. 6 in all brain voxels, and then a global k_2^r value is determined by taking the median value of k_2^r from all voxels except the reference region and voxels with very low BP. Finally, SRTM is applied to estimate BP and R_1 for all brain voxels by fixing the k_2^r value. Rapid calculation of functional images for SRTM2 was also performed by BFM in the same way as for SRTM. Wu et al. reported that the global mean of k_2^r was slightly biased (2%–6%), but the median was unbiased (<1%) and was used as the global value, and that the percent reduction in BP variation using SRTM2 compared with SRTM was 14%, 20%, and 10% for [^{18}F]FCWAY, [^{11}C]flumazenil, and [^{11}C]raclopride simulation study of 60-min scans, respectively. The magnitude of the improvement depends on

the tracer's kinetics. They concluded that SRTM2 would be a useful method to reduce noise in functional receptor imaging.

As the conclusion of this section, the SRTM with NLS is useful in ROI-based analysis because the estimation time is bearable for application to several ROI-derived TACs, there are few outliers at this noise level, and no parameter setting is required. In voxel-based estimation, SRTM with BFM is practical because this method is computationally much faster and does not give an unreasonable value. The reliability of BP estimates by SRTM depends on the tracer, and when the COV of estimates is large, the reduction of parameter number with SRTM2 is worth consideration.

Graphical analysis

The graphical analysis of Logan without arterial input function yields the distribution volume ratio (DVR) of the target to the reference tissue [25]. It uses the radioactivity concentration of the reference tissue without specific binding C_r, and k_2 value of the reference tissue (k_2^r) to eliminate the plasma integral of Eq. 3. The equation of this graphical analysis is given by

$$\frac{\int_0^T C_t(t)\mathrm{d}t}{C_t(T)} = V_R\left(\frac{\int_0^T C_r(t)\mathrm{d}t}{C_t(T)} + \frac{C_r(T)/k_2^r}{C_t(T)}\right) + b \quad \text{for} \quad t > t^* \tag{7}$$

$$V_R = \frac{V_T}{V_T^r} = \frac{\frac{K_1}{K_2}\left(1+\frac{k_3}{k_4}\right)}{\frac{k_1^r}{k_2^r}} \tag{8}$$

The relation holds only after equilibration time t^*, V_R and b are estimated as a slope and an intercept, respectively, by using points after t^*. V_R represents the DVR of the target (V_T) to reference tissue (V_T^r), and if the two-tissue compartment model is assumed for the target region, V_R can be expressed as Eq. 8. This method needs k_2^r value as an input parameter, and so it is necessary to determine the k_2^r value according to the tracer. In general, this value is determined from the average k_2^r in the reference region estimated in advance with the NLS method using the one-tissue compartment model and arterial input function. In the case of k_2^r being very different among individuals or diseases, determination of the input k_2^r value would require some caution.

If the radioactivity ratio between target and reference tissue becomes reasonably constant after t^*, DVR can also be estimated without the use of k_2^r with Eq. 9 [25]:

$$\frac{\int_0^T C_t(t)\mathrm{d}t}{C_t(T)} = V_R\frac{\int_0^T C_r(t)\mathrm{d}t}{C_t(T)} + b' \quad \text{for} \quad t > t^* \tag{9}$$

Meanwhile, in a multilinear reference tissue model (MRTM0), k_2^r is also estimated by LLS [30]. In this method, three parameters, V_R, V_R/k_2^r, and b are estimated with Eq. 10:

$$\frac{\int_0^T C_t(t)\mathrm{d}t}{C_t(T)} = V_R\frac{\int_0^T C_r(t)\mathrm{d}t}{C_r(T)} + \frac{V_R C_r(T)}{k_2^r C_t(T)} + b \quad \text{for} \quad t > t^* \tag{10}$$

LGA without arterial input function is simple, it is stable, and computer time is short as well. However, there are also two drawbacks: noise-induced bias and the determination of t^* the same as LGA with arterial input function. The statistical noise in PET data introduces a bias, and several strategies have been proposed to reduce this noise-induced bias by rearranging the equation of (7) or (10) to multilinear form, called MRTM2 and MRTM, respectively [31].

In these methods on the basis of LGA, BP or V_T cannot be estimated directly, but they can be estimated from BP = $V_R - 1$ on the assumption that K_1/k_2 of the target and reference region is equal, as is also used in SRTM. For some tracers, this assumption is not feasible, e.g., according to the heterogeneity of nonspecific binding, and in this case, in the strict sense, absolute assessment of BP is difficult [32].

Ichise et al. [31] compared the bias and variability of these methods in serotonin transporter ligand [^{11}C]DASB studies, and reported that the bias of MRTM0 was much larger than others although the COV was smallest. MRTM and SRTM reduced the bias, but then COV was large. Thereafter, this large COV was reduced in MRTM2 and SRTM2 by fixing k_2^r. Although the determination of k_2^r is necessary in these methods, they are useful for voxel-based estimation.

Models described in this section are summarized in Table 2.

Parameter estimation in irreversible model

[^{18}F]2-fluoro-2-deoxy-D-glucose (FDG) has been used widely to quantify the cerebral metabolic rate of glucose (CMRGlc, mg/min/100 g) and the individual rate constant parameters. The kinetic model for FDG is based on the two-tissue compartment model as shown in Fig. 1 [33, 34], and if the dephosphorylation is ignored, i.e., k_4 is assumed to be zero, this compartment model becomes irreversible. It has been reported that a three-